IEEE Access
Multidisciplinary | Rapid Review | Open Access Journal

Received February 1, 2020, accepted February 15, 2020, date of publication February 20, 2020, date of current version March 2, 2020.

Digital Object Identifier 10.1109/ACCESS.2020.2975126

Zero-Sequence Current Suppression for Open-Winding Permanent Magnet Brushless Motor Driving System Based on Second Order Generalized Integrator

QING LU[1,2], YUEFEI ZUO[2], TAO ZHANG[1], AND LIHONG MO[1]

[1]Faculty of Automation, Huaiyin Institute of Technology, Huai'an 223003, China
[2]School of Electrical and Information Engineering, Jiangsu University, Zhenjiang 212013, China

Corresponding author: Qing Lu (tsinglu@126.com)

This work was supported in part by the Natural Science Foundation of China under Grant 51807080, in part by the Natural Science Foundation of Jiangsu Province under Grant BK20181481, in part by the Postdoctoral Science Foundation of China under Grant 2017M610295, in part by the Six Categories Talent Peak of Jiangsu Province under Grant 2019-GDZB-238 and Grant 2016-GDZB-009, in part by the Natural Science Foundation of Huaian City under Grant HAB201832 and Grant HAB201705, and in part by the Huaian Key Laboratory of motion control and converter technology under Grant HAP201903.

ABSTRACT The open-winding driving system can improve power density and torque output capacity of the motor. However, the open-winding topology with a common direct current (DC) power supply provides a path for the zero-sequence current, which contributes to the power loss but not the torque output. The zero-sequence current is produced by the common-mode voltage and zero-sequence components of the back electromotive force (EMF). For the purpose of eliminating the common-mode voltage as well as improving the utilization of DC supply voltage, a 120° decoupling space vector pulse width modulation strategy is adopted. Meanwhile, a proportional unit combined with second order generalized integrator (SOGI) is proposed to suppress the zero-sequence current caused by the zero-sequence components of the back EMF. A test bench is built for the experiment. The effectiveness of the proposed suppression strategy is verified by the experimental results.

INDEX TERMS Electric machines, permanent magnet machines, open-winding motor, zero-sequence current suppression.

I. INTRODUCTION

Permanent magnet synchronous motor (PMSM) has been widely used in the field of electric vehicle driving and industrial applications due to its advantageous features, such as small size, low cost, high power density, and high efficiency [1]–[5]. In recent years, the price of rare-earth magnet material used in the permanent magnet (PM) motors has experienced huge fluctuations due to market monopoly and the unstable supply. Therefore, a new class of non-rare-earth PM motors that do not employ rare-earth PM material have been paid much attention. For example, the non-rare-earth and hybrid PM material brushless motors have been highlighted and reported in [6]–[10]. Because of the complex characteristics of the non-rare-earth PM material in this kind of machine, how to improve the performance of the non-rare-earth motors and hybrid permanent magnet material motors including wide speed operation, high power density, and high reliability, has become to be the cutting edge in the field of motor control.

Compared with the conventional star-connected three-phase winding, the open-winding configuration is more suitable for the non-rare-earth and hybrid magnet material PM motors due to the merits of higher efficiency, smaller capacity of the single converter and better fault-tolerant capability [11]–[14]. Generally, the open-winding motor driving system provides two kinds of power supply topology, namely, single direct current (DC) power supply and dual isolated DC power supply. Compared with the dual isolated DC power supply system, the single DC power supply based

The associate editor coordinating the review of this manuscript and approving it for publication was Atif Iqbal.

open-winding driving system is more widely used due to the advantages of simple driving system structure and relatively low cost [15]. However, the single DC power supply topology provides a path for zero-sequence current, which contributes to the additional energy loss and reduces the efficiency of driving system [16], [17]. Therefore, the suppression of zero-sequence current is very necessary.

Numerous results have been published by scholars in related fields all over the world [18]–[22]. Reference [23] proposed a method of using a series reactor to increase zero-sequence impedance, while the zero-sequence current cannot be completely suppressed by series reactor and the volume and cost of the system will be increased. Additionally, the loss will be brought to the system in practical application. In [24], the zero-sequence current is suppressed by changing the neutral point with auxiliary switches, which complicates the system structure. In [25], the space voltage vectors without common-mode voltage are selected for driving the induction motors. For PMSM with zero-sequence harmonic in the motor back electromotive force (EMF), the zero-sequence current cannot be effectively suppressed just by selecting the space voltage vectors without common-mode voltage. In [26], the proportional resonance controller in a closed loop control strategy is designed to suppress zero-sequence current of motor winding. The common-mode voltage generated by the inverter and the zero-sequence current component caused by back EMF harmonics of PMSM can be effectively suppressed. However, the structure of proportional resonance controller is complex, and the parameters are difficult to tune. In [27], a full-order adaptive zero-sequence observer is proposed to predict zero-sequence voltage and zero-sequence current. And then a novel deadbeat predictive current control method is proposed to suppress the zero-sequence current. The effectiveness of the proposed scheme is verified. However, there exists problem of large computation. Therefore, it is still a great challenge to design a method that is suitable for eliminating the zero-sequence current effectively.

Previous studies have shown that the proportional and second order generalized integrator (SOGI) controller has a large gain in a small range near the resonant frequency point, and it also has a good frequency adaptive characteristic [28]. Therefore, the proportional and SOGI regulator is more suitable for controlling specific order harmonic current. Because of the good performance, SOGI has been widely applied in many fields. In [29], [30], SOGI is adopted to suppress harmonic current in power system. In [31], SOGI is employed to suppress specific harmonics for the high speed sensorless controlled motor. In [32], SOGI is used to improve the performance of high frequency current control for low speed sensorless control motor. Consequently, SOGI is a good candidate for closed loop control of the zero-sequence current.

The main purpose of this paper is to propose an effective zero-sequence current suppression strategy for the open-winding motor. Firstly, the structure of open-winding motor is presented. Secondly, the mathematical model of the open-winding motor including the 0-axis equation is introduced. Particularly, a decoupling space vector pulse width modulation (SVPWM) is adopted to eliminate the common-mode voltage. Then, the proportional and SOGI regulator is used to suppress the zero-sequence current for the open-winding motor. Finally, experimental platform is built to validate the effectiveness of the proposed control strategy.

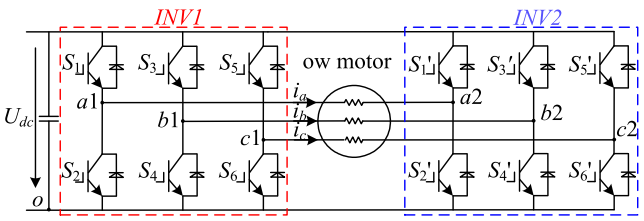

FIGURE 1. Topology structure of open-winding motor.

II. TOPOLOGY OF THE OPEN-WINDING MOTOR

According to the DC power supply mode of the two inverters, the driving system of open-winding motor is divided into two categories: single DC power supply mode, i.e. common DC bus power supply mode; dual DC power supply mode, that is, isolated DC bus power supply mode.

The topology of open-winding motor driving system with single DC power supply mode is shown in Fig. 1. It can be seen from the figure that two inverters share a common DC power supply. Compared with the structure of dual DC power supply mode, single DC power supply mode saves system cost and space.

The back EMF waveforms and spectrum analysis of the open-winding motor at 1200 r/min are shown in Fig. 2 [33]. From the Fig. 2 (a), it can be seen that the waveform is symmetrical, but the back EMF exhibits non-sinusoidal. The spectrum analysis of the back EMF waveform is shown in Fig. 2 (b). From the analysis results, it can be seen that the waveform mainly contains third and ninth harmonics and it takes up 2.62% and 5.99%, respectively. And the other orders harmonics can be neglected. That is, it is very necessary to suppress the third and ninth harmonics.

III. MATHEMATICAL MODEL OF THE OPEN-WINDING MOTOR

The topology of open-winding motor driving system with common DC bus is shown in Fig.1, namely, the neutral point of the traditional star-connected windings is opened. The opening three-phase stator windings can be supplied by the common DC bus. The two DC sides of the converter are connected to the single DC power supply.

The mathematical model of the open-winding motor can be expressed as follows:

$$\begin{bmatrix} u_a \\ u_b \\ u_c \end{bmatrix} = \begin{bmatrix} R & 0 & 0 \\ 0 & R & 0 \\ 0 & 0 & R \end{bmatrix} \begin{bmatrix} i_a \\ i_b \\ i_c \end{bmatrix} + L\frac{d}{dt}\begin{bmatrix} i_a \\ i_b \\ i_c \end{bmatrix} - \begin{bmatrix} e_a \\ e_b \\ e_c \end{bmatrix} \quad (1)$$

where, u_a, u_b and u_c represent the phase voltage; i_a, i_b and i_c represent the phase current; e_a, e_b and e_c represent the

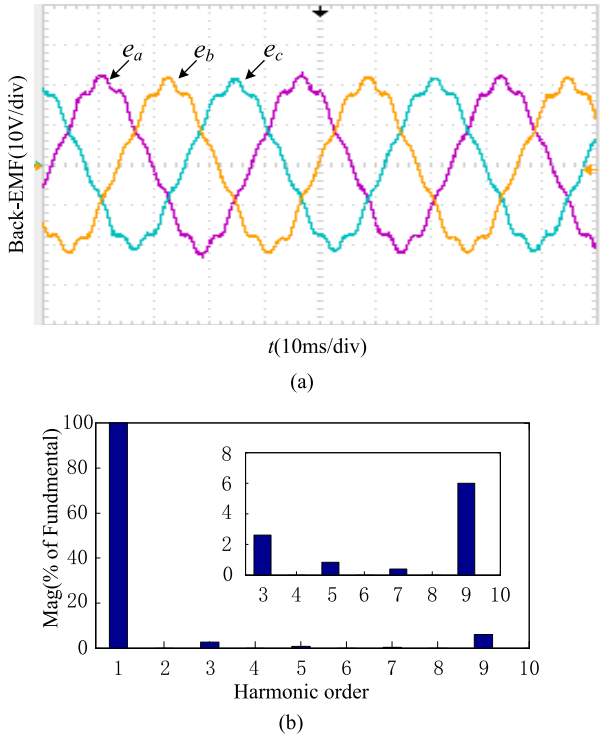

FIGURE 2. Back EMF and spectrum analysis (a) Back EMF waveforms of the motor (b) Fast Fourier Transform analysis.

phase back EMF; R is the phase resistance; L is the phase inductance.

In order to analysis the zero-sequence current, (1) can be transformed to the synchronous rotating coordinate system. Therefore, the mathematical model of motor can be rewritten as:

$$\begin{bmatrix} u_d \\ u_q \\ u_0 \end{bmatrix} = \begin{bmatrix} R & -\omega L_q & 0 \\ \omega L_d & R & 0 \\ 0 & 0 & R \end{bmatrix} \begin{bmatrix} \mathrm{i}_d \\ i_q \\ i_0 \end{bmatrix} + \begin{bmatrix} L_d & 0 & 0 \\ 0 & L_q & 0 \\ 0 & 0 & L_0 \end{bmatrix} \frac{d}{dt} \begin{bmatrix} \mathrm{i}_d \\ i_q \\ i_0 \end{bmatrix} + \begin{bmatrix} 0 \\ \omega\psi_{f1} \\ e_0 \end{bmatrix} \quad (2)$$

where, u_d, u_q and u_0 represent the phase voltage in d, q, 0 coordinate frame, respectively; i_d, i_q and i_0 represent the phase current; ω represents the electric angular frequency; e_0 is zero-sequence component of the back EMF, and ψ_{f1} is fundamental component of the rotor flux linkage.

It can be seen from (2) that there is zero-sequence current in the motor winding, if the system contains the common-mode voltage or zero-sequence component of back EMF. Therefore, the system zero-sequence current can be suppressed by the strategy of eliminating common mode voltage and compensating zero-sequence component of back EMF.

IV. COMMON MODE VOLTAGE SUPPRESSION BY 120 DEGREE DECOUPLING MODULATION

There are 64 switching states of dual-inverter in the open-winding motor driving system, and 19 effective space voltage vectors are output by 64 switching states. The open-winding motor driven by dual-inverter generates common-mode voltage, which is defined as follows:

$$\begin{aligned} u_0 &= \frac{u_{a1a2} + u_{b1b2} + u_{c1c2}}{3} \\ &= \frac{u_{a1o} - u_{a2o} + u_{b1o} - u_{b2o} + u_{c1o} - u_{c2o}}{3} \end{aligned} \quad (3)$$

It can be seen from (3) that the common-mode voltage of the dual-inverter driving system is caused by the difference of the common-mode voltage produced by each inverter. By taken the synthesized space voltage vector 12'(100110) as an example, the common-mode voltage output from inverter 1 can be expressed as follows:

$$u_{01} = \frac{u_{a1o} + u_{b1o} + u_{c1o}}{3} = \frac{U_{dc} + 0 + 0}{3} = \frac{U_{dc}}{3} \quad (4)$$

Meanwhile, the common-mode voltage output from inverter 2 can be expressed as:

$$u_{02} = \frac{u_{a2o} + u_{b2o} + u_{c2o}}{3} = \frac{U_{dc} + U_{dc} + 0}{3} = \frac{2U_{dc}}{3} \quad (5)$$

The total output common-mode voltage of the dual-inverter driving system can be obtained by substituting (4) and (5) into (3).

$$u_0 = u_{01} - u_{02} = -\frac{U_{dc}}{3} \quad (6)$$

It can be seen from (6) that the output common-mode voltage of the dual-inverter is $-U_\mathrm{dc}/3$, if the space voltage vector 12' is selected. Similarly, for other effective space voltage vectors, the common-mode voltage of the dual-inverter driving system is not zero, when the difference between the common-mode voltage of the inverter 1 and inverter 2 is not zero.

According to the idea of traditional decoupling space voltage vector, decoupling modulation strategy can modulate two inverters separately. A voltage vector $\boldsymbol{u}_{ref}$ is decomposed into two space voltage vectors $\boldsymbol{u}_{ref1}$ and $\boldsymbol{u}_{ref2}$ with equal amplitude and opposite phase. The two voltage vectors are modulated by inverter 1 and inverter 2 respectively. Then the corresponding relationship of the space voltage vector can be expressed as follows

$$u_{ref} = u_{ref1} - u_{ref2} \quad (7)$$

The voltage vector synthesis of arbitrary angle decoupling modulation is shown in Fig. 3. θ is the angle between the voltage vector u_{ref} and the α axis. The angle between the voltage vector u_{ref1} and u_{ref2} is defined as the decoupling angle γ. δ is the angle between the voltage vector $\boldsymbol{u}_{ref}$ and $\boldsymbol{u}_{ref1}$, and $\delta = (180° - \gamma)/2$. The system voltage vector $\boldsymbol{u}_{ref}$ can be decomposed into $\boldsymbol{u}_{ref1}(|u_{ref1}| \angle(\theta - \delta))$ and $\boldsymbol{u}_{ref2}(|u_{ref2}| \angle(\theta + \delta - \pi))$. The relationship between the magnitude of $\boldsymbol{u}_{ref1}$, $\boldsymbol{u}_{ref2}$, $\boldsymbol{u}_{ref}$ and the angle δ can be expressed as

$$|u_{ref1}| = |u_{ref2}| = \frac{|u_{ref}|}{2\cos\delta} \quad (8)$$

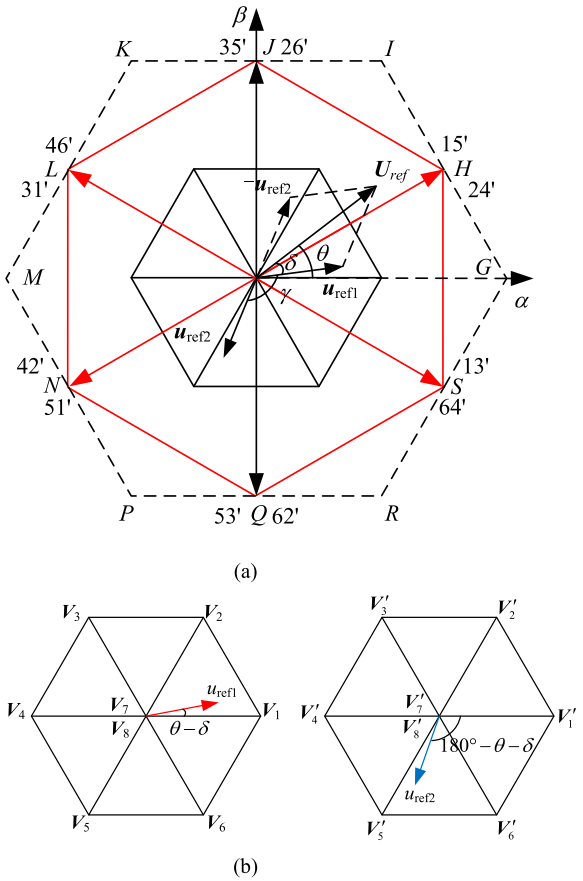

FIGURE 3. Space voltage vector of decoupling modulation (a) Voltage vector synthesis (b) Decomposition of voltage vector.

For decoupling modulation strategy, different modulation waves will be obtained when different values of decoupling angle are taken, and each waveform will be distorted to varying degrees. By comparing and analyzing the modulation waves with different decoupling angles, it can be seen that the phase voltage modulation wave is a standard sinusoidal wave when the decoupling angle is 120-degree, that is, the modulation wave as shown in Fig. 4 does not contain harmonics. Otherwise, the modulation wave contains harmonic components.

In order to further analyse the harmonic components in the modulation wave, the frequency spectrum of $f(\theta)$ is analysed. By Fourier transform, the $f(\theta)$ can be written as

$$f(\theta) = \frac{4\cos\delta}{\sqrt{3}}\cos\theta - \sum_{k=0}^{\infty}\frac{3\cos[(2k+1)3\delta]}{\pi(3k+1)(3k+2)}\cos[(2k+1)3\theta] \quad (9)$$

It can be seen from (9) that the phase voltage modulation wave contains fundamental component and odd multiple of 3 harmonics. This voltage modulation wave will lead to zero-sequence current in the winding supplied by a single DC power. If $\delta = 30°$ and the angle of decoupling $\gamma = 120°$, the harmonic value is zero, i.e., the phase voltage modulation

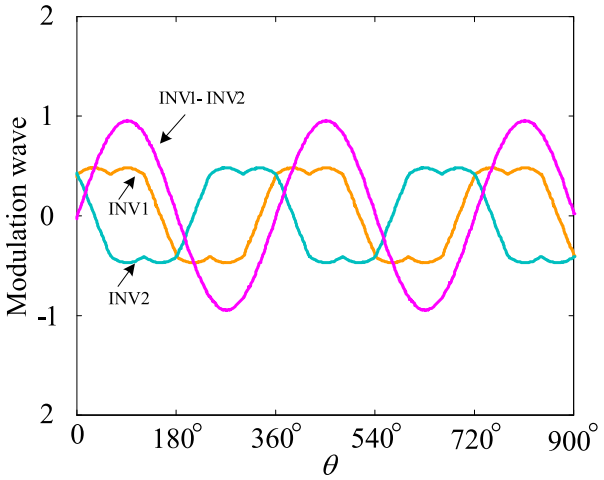

FIGURE 4. Modulation wave with 120° decoupling angles.

wave does not contain harmonic components. Therefore, the zero-sequence voltage can be eliminated by using 120-degree decoupling modulation.

If the 120-degree decoupling modulation is adopted, the voltage vector $\boldsymbol{u}_{ref}$ of the system can be decomposed into two voltage vectors with equal magnitude and 120-degree phase difference. The voltage vectors can be expressed as $\boldsymbol{u}_{ref1}(|\boldsymbol{u}_{ref1}|\angle(\theta - 30°))$ and $\boldsymbol{u}_{ref2}(|\boldsymbol{u}_{ref2}|\angle(\theta - 150°))$. According to (8), the magnitude relationship between voltage vector $\boldsymbol{u}_{ref1}$, $\boldsymbol{u}_{ref2}$ and $\boldsymbol{u}_{ref}$ can be expressed as follows

$$|u_{ref1}| = |u_{ref2}| = \frac{|u_{ref}|}{\sqrt{3}} \quad (10)$$

V. ZERO-SEQUENCE CURRENT SUPPRESSION STRATEGY OF THE OPEN-WINDING MOTOR

A. PROPORTIONAL AND SOGI REGULATOR

Since the third and ninth harmonics exist in the stator wingdings, the corresponding regulator is designed to control the zero-sequence current. The traditional proportional and integral regulator can achieve good control performance of regulating the DC component, but it cannot regulate the AC component effectively. To suppress the third and ninth harmonics, the proportional and SOGI regulator are consequently adopted to control the zero- sequence current.

The structure of SOGI is shown as Fig.5 (a). Obviously, the SOGI consists of a proportional unit and two integral units. The input signal $\omega 0$ is the basic frequency of the selective signal to be adjusted. The frequency can be multiplied by appropriate coefficient as required, such as 3 and 9. The output signal of SOGI is the component of the input signal $x_{(t)}$ at k times of basic frequency. The SOGI can work as a band-pass filter when setting $x_{0(t)}$ as the output signal. If the signal ε is set as the output, the SOGI is a band-stop filter. The performance of SOGI depends on the setting of the coefficients. In the proposed proportional and SOGI regulator, the SOGI is set as a band-pass filter [27]. The transfer

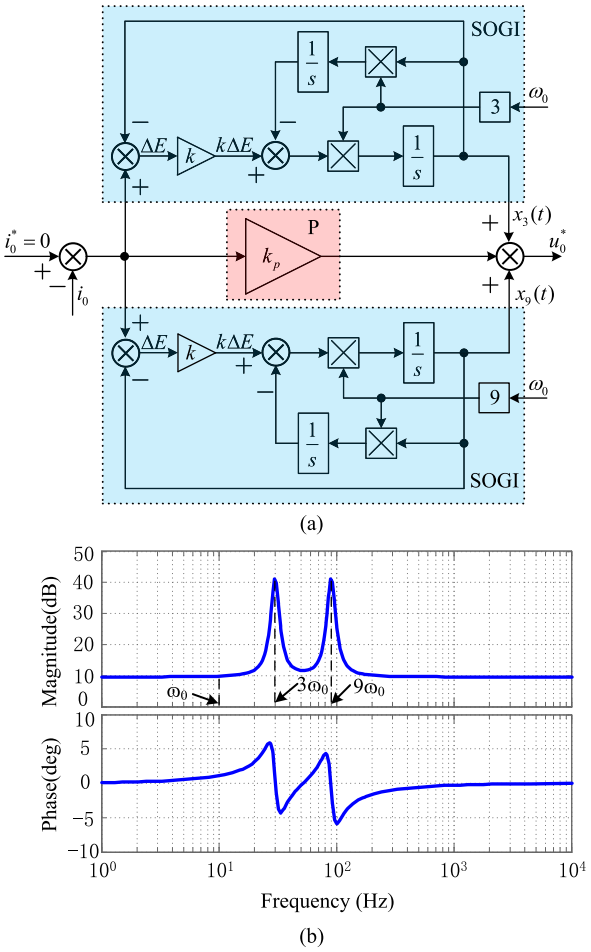

FIGURE 5. Configuration and frequency response of proportional and SOGI regulator (a) Configuration of the proposed regulator (b) Frequency response of the proposed regulator.

function of SOGI is given as follows:

$$H(s) = \frac{k\omega_0 s}{s^2 + k\omega_0 s + \omega_0^2} \tag{11}$$

Considering the third and ninth harmonics, the regulator is designed according to the harmonic orders. The detailed structure of the regulator is shown as Fig.5 (a), and the function can be expressed as:

$$H(s) = k_p + \frac{k(3\omega_0)s}{s^2 + k(3\omega_0)s + (3\omega_0)^2} + \frac{k(9\omega_0)s}{s^2 + k(9\omega_0)s + (9\omega_0)^2} \tag{12}$$

where, k_p is the proportional coefficient, k is the internal gain of SOGI. In the following simulation and experiment, the value of kp is 5 and k is 2. ω_0 is the basic frequency which is changed with speed.

The frequency response of proportional and SOGI regulator is shown as Fig.5 (b). It can be seen from the figure that the proposed regulator can achieve multiple-point resonant. It is obvious that the gain is large at the frequencies $3\omega_0$ and $9\omega_0$. The regulator can control the AC component.

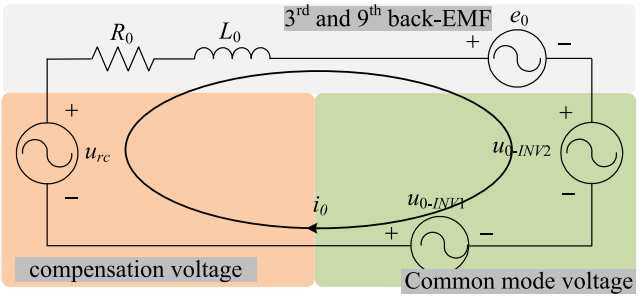

FIGURE 6. Zero sequence equivalent circuit of open-winding motor system.

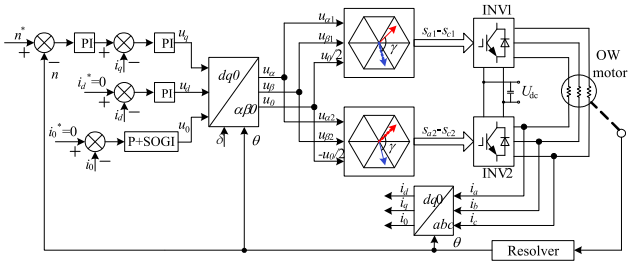

FIGURE 7. Zero-sequence current suppression system based on proportional and SOGI regulator.

B. ZERO-SEQUENCE CURRENT SUPPRESSION STRATEGY BASED ON PROPORTIONAL AND SOGI REGULATOR

Considering the third and ninth harmonics of the back EMF, the 0-axis equation in zero-sequence circuit can be expressed as:

$$u_0 = Ri_0 + L_0\frac{di_0}{dt} - 3\omega\psi_{f3}\sin 3\theta - 9\omega\psi_{f9}\sin 9\theta \tag{13}$$

Based on the above formula, it can be achieved that the zero- sequence current is generated by two major factors: the common-mode voltage resulted from the modulation mode and the zero-sequence back EMF of the motor. In order to suppress the zero-sequence current efficiently, as shown in Fig.6, a zero-sequence compensation voltage is inserted into the zero-sequence circuit. As a result, the sum of the voltage sources in the circuit is zero.

The u_{0-INV1} and the u_{0-INV2} are generated by inverter-1 and inverter-2, respectively; the $3\omega\psi_{f3}\sin 3\theta$ and the $9\omega\psi_{f9}\sin 9\theta$ are generated by the zero-sequence back EMF; the u_{rc} is the zero-sequence compensation voltage.

Based on the above analysis, the modulation strategy and closed loop compensation strategy can be used together to suppress zero-sequence current.

As shown in Fig. 7, the vector control system of open winding motor with zero-sequence current suppression strategy is designed. The 120-degree decoupling modulation is used to eliminate common-mode voltage. In the zero-sequence current circuit, the given value of current is zero, and the zero-sequence current is suppressed by proportional and SOGI regulator.

VI. EXPERIMENTAL VALIDATION

In order to further verify the effectiveness of the 120- degree decoupling modulation strategy and the

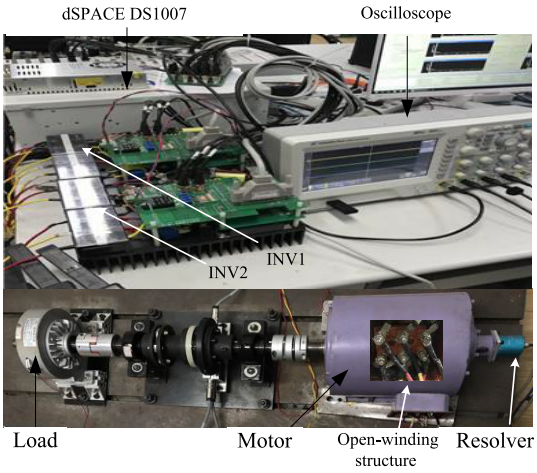

FIGURE 8. Experimental platform of open-winding motor drive system.

TABLE 1. The motor parameters.

Parameter/Unit	Value
Rated power /kW	2.5
pole pairs	5
Ld /mH	3.707
Lq /mH	5.308
PM flux/Wb	0.129
phase resistance/Ω	0.239

zero-sequence current suppression strategy based on proportional and SOGI regulator, an experimental platform for the open-wingding motor is established and shown in Fig. 8. Here, DS1007 dSPACE is used as the main controller of the experimental platform. The controller can execute the control algorithm, and generate 12 PWM driving signals to drive the dual-inverter. Two independent inverters are applied in the main circuit. And the inverters are powered by a single DC power supply. The magnetic powder brake is used for loading and unloading. The speed and rotor position of the motor are detected by a resolver installed on motor shaft. The switching frequency is 10 kHz. The motor parameters are shown in table 1.

All the experimental results are taken when the inverters are switched with the modulation scheme for common-mode voltage suppression. The zero-sequence current suppression performance of the proposed regulator is compared with that of the traditional regulator. The experimental results show the steady-state performance of the motor at constant speed, the speed tracking performance with speed variations and the disturbance rejection ability under load variation, respectively. Furthermore, the performance of zero- sequence current suppression of the 120-degree decoupling modulation

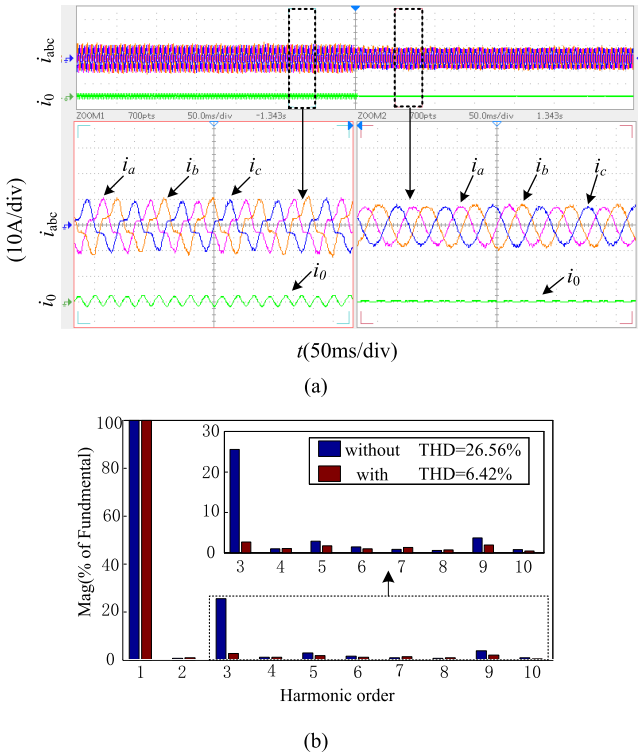

FIGURE 9. Current waveform and spectrum analysis of steady state (a) Currents of steady state without and with proportional and SOGI regulator (b) The spectrum analysis of a-phase current.

strategy and the proposed proportional and SOGI regulator are verified.

A. ANALYSIS OF STEADY-STATE EXPERIMENTAL RESULTS

Firstly, the performance of zero-sequence current suppression based on proportional and SOGI regulator is analyzed experimentally in steady state. The three-phase current, zero-sequence current waveform and phase current spectrum analysis results of open-winding motor without and with the proposed regulator are shown in Fig. 9.

Fig. 9(a) shows the comparison waveforms of current, and which are conducted without and with the proposed regulator under the rated load at 100r/min. From the results, it can be seen that the three-phase current distortion is serious and the zero-sequence current reaches 2.5A without the zero-sequence current suppression strategy. It is obviously that the three-phase current waveform becomes more sinusoidal with the contribution of the proposed proportional and SOGI regulator. Simultaneously, the zero-sequence current is reduced from 2.5A to 0.5A.

Fig. 9 (b) shows the Fast Fourier Transform (FFT) analysis results of the phase-a current. It can be seen that the third and ninth harmonics account for 25.50% and 3.68% without the proposed regulator. Nevertheless, in the case of regulator, the third and ninth harmonic contents are only 2.68% and 1.89%. The total harmonic distortion rate of the phase current is reduced from 26.56% to 6.42%.

From the comparison and analysis of the experimental results, it can be achieved that the proposed control method

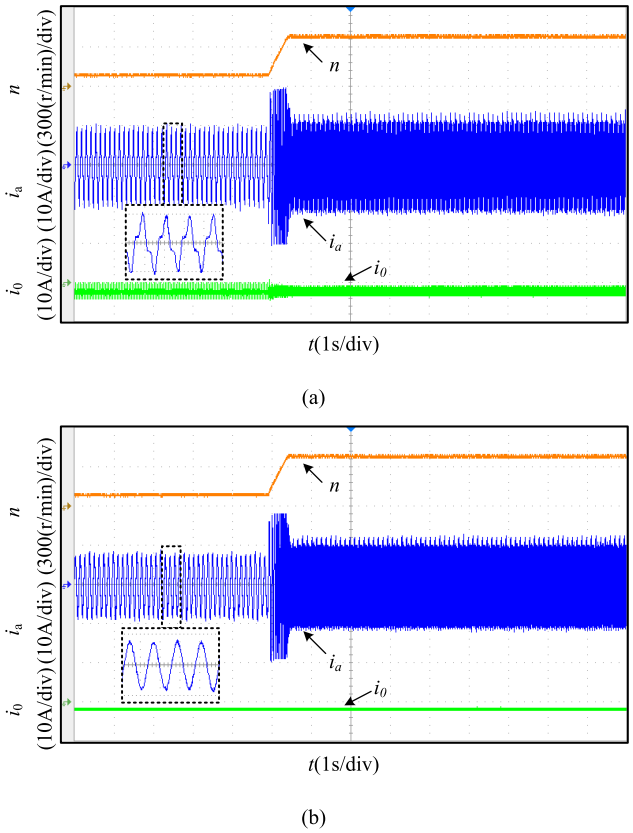

FIGURE 10. Zero-sequence current suppression effect under speed changed (a) without proposed regulator (b) with proposed regulator.

based on the proposed regulator can effectively suppress the zero-sequence current in steady-state.

B. ANALYSIS OF DYNAMIC-STATE EXPERIMENTAL RESULTS

In order to verify the performance of zero-sequence current suppression based on proportional and SOGI regulator in dynamic state, the waveforms of the driving system without and with the proposed regulator are given in Fig. 10 and Fig.11.

The speed tracking ability with proportional and SOGI controller is demonstrated in Fig. 10. The results show that dynamic response time is 200ms from 100r/min to 400r/min. From top to bottom, the waveforms are motor speed, phase-a current and zero-sequence current, respectively.

Fig. 10(a) shows the speed and current waveforms without proportional and SOGI regulator, and Fig. 10(b) is the experimental results with proportional and SOGI regulator. Based on the two methods, it can be seen from the curves that the proposed zero-sequence current suppression strategy can effectively suppress the zero-sequence current in the process of speed varied from 100 r/min to 400 r/min, and the constant speed.

In order to further verify the effectiveness of the proportional and SOGI regulator in dynamic state, the experimental results of open-winding motor driving system under

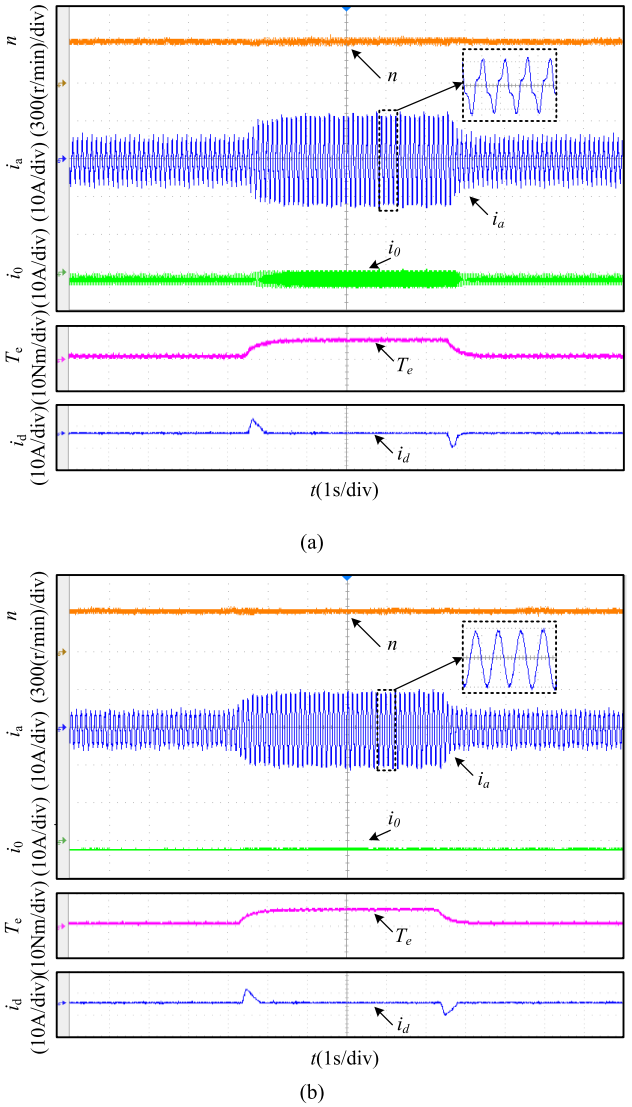

FIGURE 11. Zero-sequence current suppression under load changed (a) without proposed regulator (b) with proposed regulator.

load disturbance are given in Fig. 11. Here, the load is suddenly increased from 0Nm to 6Nm, and then reduced to 0Nm at 300r/min. The experimental waveforms of two methods are shown in Fig. 11(a) and (b). From top to bottom, the curves are motor speed, phase-a current, zero-sequence current waveforms, motor torque and the d-axis current, respectively.

From the experimental results of Fig. 11(a), it can be seen that the phase-a current and zero-sequence current increase obviously when the load changes from 0Nm to 6Nm, in the case that without zero-sequence current suppression strategy. When the proportional and SOGI regulator is enabled, the zero-sequence current kept a very small value as shown in Fig. 11(b). From the comparison of Fig. 11 (a) and Fig. 11(b), the same conclusion can be drawn that the proposed control strategy exhibits good ability of zero-sequence current suppression when the load changes abruptly. In the process of load variations, the zero-sequence current can be

kept in the range of +0.2A and −0.2A. Therefore, the disturbance rejection ability of the proposed method is verified.

The above current waveforms without and with the proposed regulator are compared and analyzed under different conditions: steady-state, speed variations and load variations. The experimental results show that the driving system with proportional and SOGI regulator not only has zero-sequence current suppression ability in steady state, but also has good performance of speed tracking and disturbance rejection. Therefore, the proposed method has good steady and dynamic performance. And the system with proportional and SOGI regulator has good performance of the zero-sequence current suppression.

VII. CONCLUSION

To suppress the zero-sequence current in the open-winding motor driving system with a common DC bus, the 120-degree decoupling modulation technique is utilized, and the proportional and SOGI regulator is proposed in this paper.

Firstly, the open-winding motor driving system with single DC power supply and the mathematical model are introduced. The space voltage vector synthesis of dual-inverter is given. Then the common-mode voltage of decoupling modulation is studied, and a 120-degree decoupling modulation strategy is adopted to suppress the common-mode voltage. Based on the analysis of the regulator performance, a control strategy of using the proportional and SOGI regulator for zero-sequence current suppression is proposed. Finally, an experimental platform based on the DS1007 dSPACE controller is built. The experimental results in both steady and dynamic states are presented. The comparison results indicate that the proposed proportional and SOGI regulator has an excellent performance of zero-sequence current suppression.

REFERENCES

[1] Z. Q. Zhu, "Overview of novel magnetically geared machines with partitioned stators," *IET Electr. Power Appl.*, vol. 12, no. 5, pp. 595–604, May 2018.

[2] M. Cheng, W. Hua, J. Zhang, and W. Zhao, "Overview of stator-permanent magnet brushless machines," *IEEE Trans. Ind. Electron.*, vol. 58, no. 11, pp. 5087–5101, Nov. 2011.

[3] X. Zhu, D. Fan, L. Mo, Y. Chen, and L. Quan, "Multiobjective optimization design of a double-rotor flux-switching permanent magnet machine considering multimode operation," *IEEE Trans. Ind. Electron.*, vol. 66, no. 1, pp. 641–653, Jan. 2019.

[4] X. Zhu, Z. Xiang, C. Zhang, L. Quan, Y. Du, and W. Gu, "Co-reduction of torque ripple for outer rotor flux-switching PM motor using systematic multi-level design and control schemes," *IEEE Trans. Ind. Electron.*, vol. 64, no. 2, pp. 1102–1112, Feb. 2017.

[5] X. Sun, C. Hu, G. Lei, Y. Guo, and J. Zhu, "State feedback control for a PM hub motor based on gray wolf optimization algorithm," *IEEE Trans. Power Electron.*, vol. 35, no. 1, pp. 1136–1146 Jan. 2020.

[6] S. J. Galioto, P. B. Reddy, A. M. EL-Refaie, and J. P. Alexander, "Effect of magnet types on performance of high-speed spoke Interior-Permanent-Magnet machines designed for traction applications," *IEEE Trans. Ind. Appl.*, vol. 51, no. 3, pp. 2148–2160, May 2015.

[7] A. Vagati, B. Boazzo, P. Guglielmi, and G. Pellegrino, "Design of ferrite-assisted synchronous reluctance machines robust toward demagnetization," *IEEE Trans. Ind. Appl.*, vol. 50, no. 3, pp. 1768–1779, May 2014.

[8] H. Hua, Z. Q. Zhu, A. Pride, R. P. Deodhar, and T. Sasaki, "A novel variable flux memory machine with series hybrid magnets," *IEEE Trans. Ind. Appl.*, vol. 53, no. 5, pp. 4396–4405, Sep. 2017.

[9] X. Zhu, Z. Xiang, L. Quan, W. Wu, and Y. Du, "Multimode optimization design methodology for a flux-controllable stator permanent magnet memory motor considering driving cycles," *IEEE Trans. Ind. Electron.*, vol. 65, no. 7, pp. 5353–5366, Jul. 2018.

[10] X. Zhu, Z. Xiang, L. Quan, Y. Chen, and L. Mo, "Multimode optimization research on a multiport magnetic planetary gear permanent magnet machine for hybrid electric vehicles," *IEEE Trans. Ind. Electron.*, vol. 65, no. 11, pp. 9035–9046, Nov. 2018.

[11] M. Chen and D. Sun, "A unified space vector pulse width modulation for dual two-level inverter system," *IEEE Trans. Power Electron.*, vol. 32, no. 2, pp. 889–893, Feb. 2017.

[12] N. K. Nguyen, F. Meinguet, E. Semail, and X. Kestelyn, "Fault-tolerant operation of an open-end winding five-phase PMSM drive with short-circuit inverter fault," *IEEE Trans. Ind. Electron.*, vol. 63, no. 1, pp. 595–605, Jan. 2016.

[13] X. Lin, W. Huang, and L. Wang, "SVPWM strategy based on the hysteresis controller of zero-sequence current for three-phase open-end winding PMSM," *IEEE Trans. Power Electron.*, vol. 34, no. 4, pp. 3474–3486, Apr. 2019.

[14] A. Somani, R. K. Gupta, K. K. Mohapatra, and N. Mohan, "On the causes of circulating currents in PWM drives with open-end winding AC machines," *IEEE Trans. Ind. Electron.*, vol. 60, no. 9, pp. 3670–3678, Sep. 2013.

[15] Z. Zhu, B. Lee, and X. Liu, "Integrated field and armature current control strategy for variable flux reluctance machine using open winding," *IEEE Trans. Ind. Appl.*, to be published.

[16] W. Jiang, W. Ma, J. Wang, W. Wang, X. Zhang, and L. Wang, "Suppression of zero sequence circulating current for parallel three-phase grid-connected converters using hybrid modulation strategy," *IEEE Trans. Ind. Electron.*, vol. 65, no. 4, pp. 3017–3026 Apr. 2018.

[17] V. T. Somasekhar, S. Srinivas, and K. K. Kumar, "Effect of zero-vector placement in a dual-inverter fed open-end winding induction-motor drive with a decoupled space-vector PWM strategy," *IEEE Trans. Ind. Electron.*, vol. 55, no. 6, pp. 2497–2505, Jun. 2008.

[18] X. Zhang and K. Wang, "Current prediction based zero sequence current suppression strategy for the semicontrolled open-winding PMSM generation system with a common DC bus," *IEEE Trans. Ind. Electron.*, vol. 65, no. 8, pp. 6066–6076, Aug. 2018.

[19] K. R. Sekhar and S. Srinivas, "Discontinuous decoupled PWMs for reduced current ripple in a dual two-level inverter fed open-end winding induction motor drive," *IEEE Trans. Power Electron.*, vol. 28, no. 5, pp. 2493–2502, May 2013.

[20] Z. Song, X. Ma, and Y. Yu, "Design of zero-sequence current controller for open-end winding PMSMs considering current measurement errors," *IEEE Trans. Power Electron.*, to be published, doi: 10.1109/TPEL.2019.2952402.

[21] X. Zhang, W. Zhang, C. Xu, Y. Li, Y. Wang, and D. Gao, "Three-dimensional vector based model predictive current control for open-end winding PMSG system with zero-sequence current suppression," *IEEE J. Emerg. Sel.Topics Power Electron.*, to be published.

[22] H. Nian, Y. Zhou, and H. Zeng, "Zero-sequence current suppression strategy for open winding PMSG fed by semicontrolled converter," *IEEE Trans. Power Electron.*, vol. 31, no. 1, pp. 711–720, Jan. 2016.

[23] T. Kawabata, E. C. Ejiogu, Y. Kawabata, and K. Nishiyama, "New open-winding configurations for high-power inverters," in *Proc. ISIE Proc. IEEE Int. Symp. Ind. Electron.*, vol. 2, Jul. 1997, pp. 457–462.

[24] V. T. Somasekhar, K. Gopakumar, A. Pittet, and V. T. Ranganathan, "PWM inverter switching strategy for a dual two-level inverter fed open-end winding induction motor drive with a switched neutral," *IEE Proc.-Electr. Power Appl.*, vol. 149, no. 2, p. 152, 2002.

[25] M. R. Baiju, K. K. Mohapatra, R. S. Kanchan, and K. Gopakumar, "A dual two-level inverter scheme with common mode voltage elimination for an induction motor drive," *IEEE Trans. Power Electron.*, vol. 19, no. 3, pp. 794–805, May 2004.

[26] Y. Zhou and H. Nian, "Zero-sequence current suppression strategy of open-winding PMSG system with common DC bus based on zero vector redistribution," *IEEE Trans. Ind. Electron.*, vol. 62, no. 6, pp. 3399–3408, Jun. 2015.

[27] X. Yuan, C. Zhang, and S. Zhang, "A novel deadbeat predictive current control scheme for OEW-PMSM drives," *IEEE Trans. Power Electron.*, vol. 34, no. 12, pp. 11990–12000, Dec. 2019.

[28] B. Liu, B. Zhou, and T. Ni, "Principle and stability analysis of an improved self-sensing control strategy for surface-mounted PMSM drives using second-order generalized integrators," *IEEE Trans. Energy Convers.*, vol. 33, no. 1, pp. 126–136, Mar. 2018.
[29] Z. Xin, X. Wang, Z. Qin, M. Lu, P. C. Loh, and F. Blaabjerg, "An improved second-order generalized integrator based quadrature signal generator," *IEEE Trans. Power Electron.*, vol. 31, no. 12, pp. 8068–8073, Dec. 2016.
[30] Y. Wang, H. Liu, X. Han, and K. Wang, "Frequency-adaptive grid-virtual-flux synchronization by multiple second-order generalized integrators under distorted grid conditions," *TURKISH J. Electr. Eng. Comput. Sci.*, vol. 23, pp. 1930–1945, 2015.
[31] L. S. Xavier, A. F. Cupertino, J. T. de Resende, V. F. Mendes, and H. A. Pereira, "Adaptive current control strategy for harmonic compensation in single-phase solar inverters," *Electr. Power Syst. Res.*, vol. 142, pp. 84–95, Jan. 2017.
[32] G. Wang, L. Ding, Z. Li, J. Xu, G. Zhang, H. Zhan, R. Ni, and D. Xu, "Enhanced position observer using second-order generalized integrator for sensorless interior permanent magnet synchronous motor drives," *IEEE Trans. Energy Convers.*, vol. 29, no. 2, pp. 486–495, Jun. 2014.
[33] X. Zhu, Z. Shu, L. Quan, Z. Xiang, and X. Pan, "Design and multicondition comparison of two outer-rotor flux-switching permanent-magnet motors for in-wheel traction applications," *IEEE Trans. Ind. Electron.*, vol. 64, no. 8, pp. 6137–6148, Aug. 2017.

QING LU received the B.S. degree from Hangzhou Dianzi University, Hangzhou, China, in 2003, the M.S. degree from the China University of Mining and Technology, Xuzhou, China, in 2008, and the Ph.D. degree in electrical engineering from Jiangsu University, Zhenjiang, China. He is currently a Lecturer with the Faculty of Automation, Huaiyin Institute of Technology. His main research interests include high-performance permanent magnet synchronous motor design and control.

YUEFEI ZUO received the B.Sc. and the Ph.D. degrees in electrical engineering and automation from the Nanjing University of Aeronautics and Astronautics, Nanjing, China, in 2010 and 2016, respectively. He is currently a Lecturer with the School of Electrical and Information Engineering, Jiangsu University. His main research interests include modeling and advanced drive control strategies for high-performance permanent magnet synchronous motor.

TAO ZHANG was born in Huai'an, China, in 1978. He received the B.S. degree in power electronic, the M.S. degree in power transmission, and the Ph.D. degree in electrical engineering from Jiangsu University, Zhenjiang, China, in 2001, 2006, and 2012, respectively. He is currently an Assistant Professor with the Huaiyin Institute of Technology. His current research interests include bearingless motors, magnetic bearings, high-speed motors, and control strategies.

LIHONG MO received the M.S. degree in electrical engineering from the Anhui University of Science and Technology, Huainan, China, in 2005, and the Ph.D. degree in electrical engineering from Jiangsu University, Zhenjiang, China, in 2015. She is currently an Assistant Professor with the Huaiyin Institute of Technology. Her research interests include permanent magnet machine design, modeling, and control.